Available online at www.sciencedirect.com
SCIENCE DIRECT®
Journal of Contaminant Hydrology 74 (2004) 39–59
JOURNAL OF Contaminant Hydrology
www.elsevier.com/locate/jconhyd

Field investigation into unsaturated flow and transport in a fault: model analyses

H.H. Liu[a,*], R. Salve[a], J.S. Wang[a], G.S. Bodvarsson[a], D. Hudson[b]

[a] *Earth Science Division, Lawrence Berkeley National Laboratory, 1 Cyclotron Road-Mailstop 90-1116, Berkeley, CA 94720, USA*
[b] *U.S. Geological Survey, Sacramento, CA, USA*

Received 4 June 2003; received in revised form 2 February 2004; accepted 6 February 2004

Abstract

Results of a fault test performed in the unsaturated zone of Yucca Mountain, Nevada, were analyzed using a three-dimensional numerical model. The fault was explicitly represented as a discrete feature and the surrounding rock was treated as a dual-continuum (fracture–matrix) system. Model calibration against seepage and water-travel-velocity data suggests that lithophysal cavities connected to fractures can considerably enhance the effective fracture porosity and therefore retard water flow in fractures. Comparisons between simulation results and tracer concentration data also indicate that matrix diffusion is an important mechanism for solute transport in unsaturated fractured rock. We found that an increased fault–matrix and fracture–matrix interface areas were needed to match the observed tracer data, which is consistent with previous studies. The study results suggest that the current site-scale model for the unsaturated zone of Yucca Mountain may underestimate radionuclide transport time within the unsaturated zone, because an increased fracture–matrix interface area and the increased effective fracture porosity arising from lithophysal cavities are not considered in the current site-scale model.

Keywords: Fault; Matrix; Fracture

1. Introduction

Understanding and modeling flow and transport processes in unsaturated fractured rock are of importance to many areas, including geological disposal of nuclear waste and

* Corresponding author. Fax: +1-510-486-5686.
E-mail address: hhliu@lbl.gov (H.H. Liu).

0169-7722/$ - see front matter © 2004 Published by Elsevier B.V.
doi:10.1016/j.jconhyd.2004.02.004

environmental contamination in arid and semiarid regions (Bodvarsson and Tsang, 1999; Pruess, 1999). These processes are generally complicated, owing to the complexity of fracture–matrix interaction, distinct differences in hydraulic properties between fractures and matrix, and nonlinearity involved in unsaturated flow (Liu et al., 1998). Model analyses of carefully designed field studies in natural fractured rocks are useful for improving our understanding of, evaluating modeling approaches to, and calibrating the relevant model parameters for these processes (e.g., Wang et al., 1999; Tsang and Birkholzer, 1999; Salve and Oldenburg, 2001; Liu et al., 2003a).

Recently, Salve et al. (2004) performed a field study of unsaturated flow and transport in a fault within the unsaturated zone of Yucca Mountain, Nevada, the proposed repository site of high-level nuclear waste in the United States. The test was carried out in the welded rock of the Topapah Spring Tuff unit (TSw), the host rock for the proposed repository to be located approximately midway between the surface and the water table (located about 600 m below ground surface). The spatial scale of the test (distance between water release and collection locations) is about 20 m. This test generated a useful data set for water flow and solute transport within the fault. To the best of our knowledge, field tests involving both water flow and solute transport within a fault under unsaturated conditions are rare in the literature. The major objective of this paper is to report on our model interpretation of these results. Note that previous studies have indicated that faults can act as important flow and transport paths in unsaturated rock (Wang and Narasimhan, 1993; Wu et al., 2002).

In this study, we give special attention to matrix diffusion because of its potential importance in retarding radionuclide transport in unsaturated rock (Bodvarsson et al., 2001; Liu et al., 2003b). While effects of matrix diffusion on solute transport in saturated fractured rocks have been intensively investigated (e.g., Neretnieks, 1980, 2002; Moreno et al., 1997; Ostensen, 1998; Jardine et al., 1999; Shapiro, 2001; McKenna et al., 2001; Meigs and Beauheim, 2001), studies of these effects in unsaturated fractured rock are relatively limited in the literature. Compared with saturated systems, the effects of matrix diffusion in unsaturated systems are more complex, owing to the involved multiphase flow processes and the corresponding fracture–matrix interaction mechanisms.

The importance of matrix diffusion in unsaturated fractured media seems to be first recognized in the course of interpreting tritium data collected from an unsaturated chalk system in southern England, as indicated by Phillips (2001). At that site, surprisingly slow tritium transport in unsaturated chalk initially created confusion. This confusion was later successfully cleared up by Foster (1975) who explained the slow tritium transport in terms of matrix diffusion. Bodvarsson et al. (2001) reported a one-dimensional, site-scale (dual-continuum) numerical study of flow and transport in the unsaturated zone of Yucca Mountain. They found that the simulated tracer breakthrough curves at the water table are largely determined by matrix diffusion in unsaturated fractured rock (and relatively insensitive to dispersivity values assigned to the fracture continuum.) They argued that large-scale dispersion results from subsurface heterogeneities, and that for a dual-continuum system, the largest heterogeneity corresponds to property differences between fractures and the matrix. As a result, the importance of heterogeneity within the fracture network (resulting in dispersion processes in the fracture continuum) becomes secondary compared with mass transport between the

two continua with distinctly different hydraulic properties. Liu et al. (2003b) presented a model analysis of an unsaturated flow and transport field test (with a spatial scale of about 30 m) within a densely fractured rock (Allan L. Flint and David Hudson, personal communication, 2002). They also found that observed tracer breakthrough curves could be largely explained by matrix diffusion, supporting the findings of Bodvarsson et al. (2001). They also acknowledged that because of some uncertainties in their modeling study, further evaluation of the importance of matrix diffusion in unsaturated fractured rock is needed. Most recently, Seol et al. (2003) reported a numerical model study of unsaturated flow and transport in a simple, discrete fracture–matrix system (with a spatial scale of about 100 m). They found that matrix diffusion is a key mechanism for retarding radionuclide transport under unsaturated conditions. The current fault test (Salve et al., 2004) provides a useful data set for evaluating the importance of matrix diffusion for solute transport in a fault and the surrounding fractured rock under unsaturated conditions.

In this paper, we first highlight the test observations used in our model study, and then present modeling approaches. This is followed by a comparison between simulation results and experimental observations, with a focus on evaluating the importance of matrix diffusion. The implications of this study for radionuclide transport in the unsaturated zone of Yucca Mountain are also discussed.

2. Field observations

While the details of the fault test are given in Salve et al. (2004), this section highlights experimental observations used in our model analyses. The test was carried out in the upper lithophysal (Tptpul) and middle nonlithophysal (Tptpmn) subunits in the unsaturated zone of Yucca Mountain (Fig. 1). These geological subunits correspond to model layers tsw33 and tsw34, respectively, in the site-scale model for the unsaturated zone of Yucca Mountain (Liu and Ahlers, 2000). Layer tsw33 has lithophysal cavities (with sizes on the order of several to tens of centimeters), some of which may intersect fractures, whereas layer tsw34 does not. Liquid water with and without tracers was applied at the floor of an alcove (Alcove 8 in Fig. 1) from an infiltration plot (about 5 m long and 0.45 m wide) along the fault within tsw33. Seepage from the fault into an underlying niche (Niche 3 in Fig. 1) and tracer concentrations of seeping liquid as a function of time were monitored. The niche is located within tsw34, about 20 m below the floor of the alcove; the interface between tsw33 and tsw34 is about 15 m below the floor of the alcove. The fault is visible at both the floor of the alcove and the ceiling of the niche.

A water-pressure head of 2 cm was applied at the infiltration plot along the fault at the alcove. The plot consists of four trenches that have different infiltration rates as a result of subsurface heterogeneity along the fault. Fig. 2 shows the total infiltration rate as a function of time. For simplicity, our model assumes a uniformly distributed infiltration rate along the infiltration plot, to be consistent with the use of a uniform property distribution in the site-scale model of the unsaturated zone of Yucca Mountain. One consideration in our modeling study is to evaluate approaches used in the site-scale

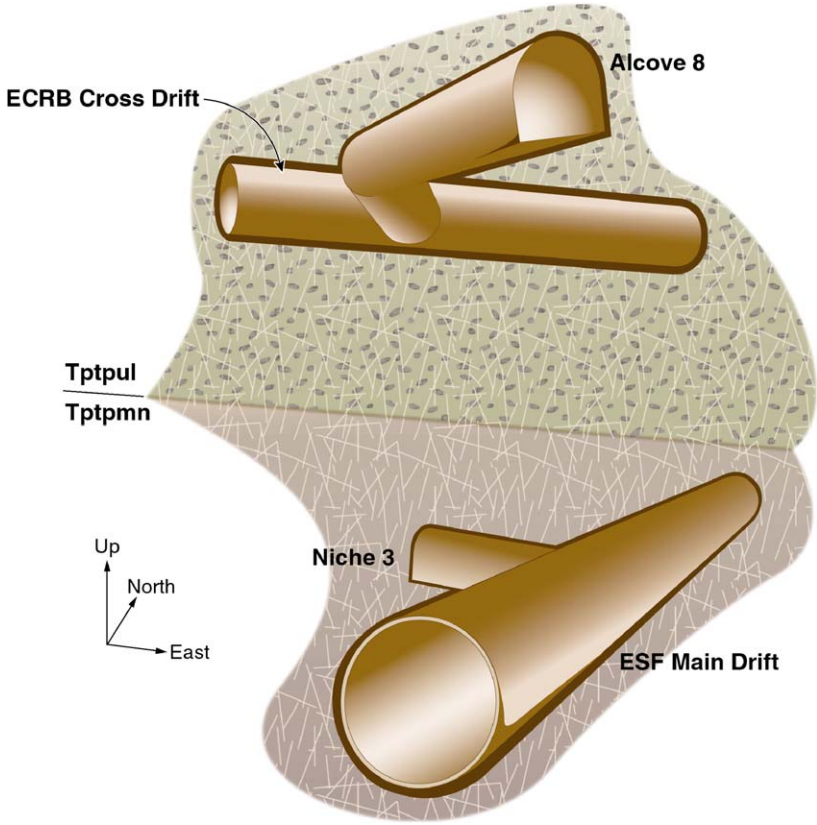

Fig. 1. Schematic illustration of the test bed for the field test. Exploratory Studies Facility (ESF) and Enhanced Characterization of Repository Block (ECRB) are underground tunnels in the unsaturated zone of Yucca Mountain.

model (Wu et al., 2002; Moridis and Hu, 2000). Previous field infiltration tests in the unsaturated zone of Yucca Mountain showed that for a given water pressure, infiltration rates usually reached constant values quickly. However, this is not the case for the recent fault test (Fig. 2). Considerable temporal variability of infiltration rate occurred during the test, as a result of infill materials within the fault just below the infiltration plot (Salve et al., 2004). In other words, the effective permeability of the fault just below the plot changed with time. It is also expected that most portions of the fault and the surrounding fractures away from the plot would still be unsaturated, although capillary pressure at the plot was positive during the test. Based on these observations and considerations, the total infiltration rate (instead of a pressure head of 2 cm) was used as the boundary condition in our model.

Seepage from the fault into the niche was measured during the test, with a number of trays used to cover the areas where seepage might occur. Seepage was found to be highly spatially variable. The total seepage rate (from all the trays) as a function of time is given

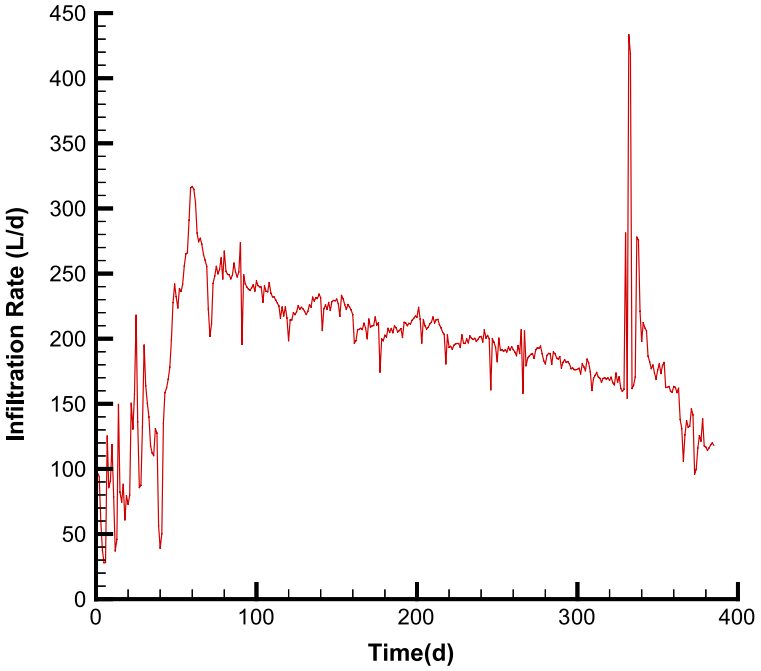

Fig. 2. Infiltration rate as a function of time (Salve et al., 2004).

in Fig. 3 (Salve et al., 2004). The recovery rate (the ratio of the total seepage collected at the niche from the fault to the total amount of water applied at the infiltration plot) is about 10% as a result of (a) water flow from the fault to the surrounding fractured rock and (b) the capillary barrier effect of the underground opening (the niche).

During the tests, three boreholes (BH8, BH9 and BH10) were installed above the niche (Fig. 4). Water arrival times at these boreholes were monitored by the electronic resistance (ER) probes (Salve et al., 2004). The arrival times were successfully monitored from Boreholes BH9 and BH10 only. Fig. 5 shows average water travel velocities determined as ratios of the distance (between the infiltration plot and the boreholes) to the arrival times from the two boreholes that are about 1 m above the ceiling of the niche. The fault is about 2 m from the borehole collars in Fig. 5. Note that relatively uniform water-travel-velocity distribution within and near the fault was observed from these two boreholes.

After 209 days, two tracers with different molecular diffusion coefficients (Br and pentafluorobenzoate (PFBA)) were introduced into infiltrating water at the infiltration plot. Tracer concentrations from three trays (at the niche) among seven trays capturing seeping water from the fault were measured (Salve et al., 2004). Seepage rates corresponding to these three trays were not measured during the period of tracer concentration measurement. In this study, a flux-averaged breakthrough curve (concentration as a function of time) from these trays was used to represent the average breakthrough curve for all trays at the niche where seepage was captured. A constant

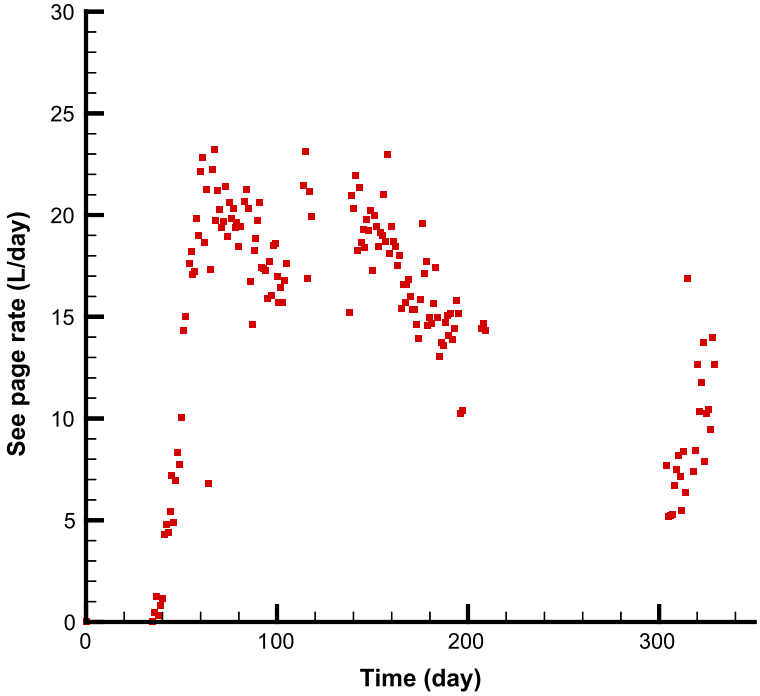

Fig. 3. Total seepage rate at the niche as a function of time (Salve et al., 2004).

flux value for each of the three trays was used to approximately determine the flux-averaged breakthrough curve (Fig. 6). The constant flux values for the three trays were determined as the averaged value over 56 days before tracers were introduced. Although uncertainties introduced by this approximation are difficult to evaluate as a result of data limitation, they are expected to be limited because not the absolute values of fluxes, but

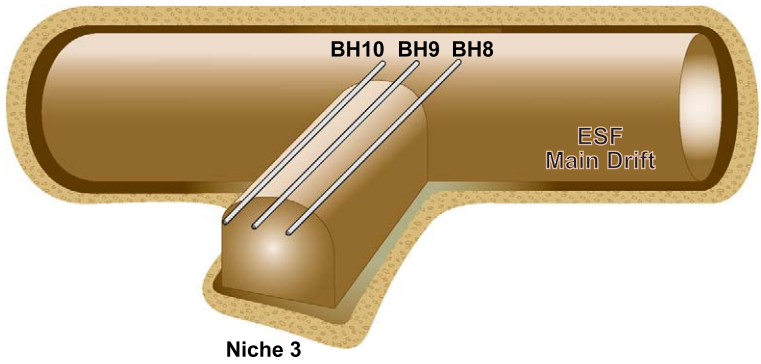

Fig. 4. Schematic illusion of the monitoring boreholes above the niche.

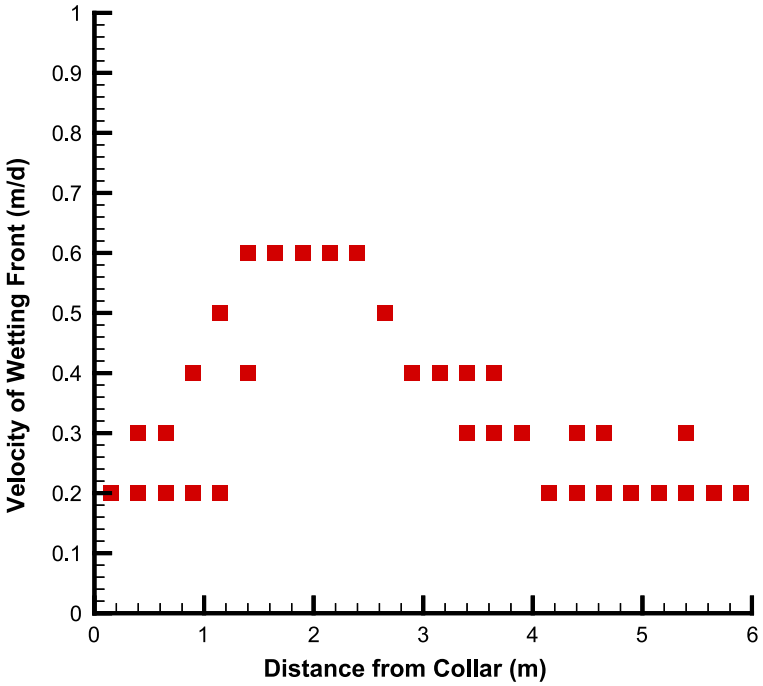

Fig. 5. Water-travel-velocity data inferred from water arrival times at boreholes (Salve et al., 2004).

the ratios between them determine the flux-averaged tracer concentration values. The flux-averaged breakthrough curve is used to compare with simulation results.

3. Numerical model

A numerical model was developed for the fault test site to compare the simulation results with the relevant field observations. While comparison results will be presented below in Section 4, here we will focus on schemes used for developing the numerical model.

A three-dimensional numerical grid was constructed for simulating the fault test (Fig. 7). The fault was represented as a vertical fracture-like feature, and the surrounding fractured rock is approximated as a dual-continuum system consisting of overlapped, interacting fracture and matrix continua. (Details of the dual-continuum approach can be found elsewhere (e.g., Doughty, 1999).) Global water flow and solute transport are allowed to occur in both continua. Fig. 7 shows a cross section of the grid within the fault. The thickness of the grid in the direction perpendicular to the fault walls is 3 m along each side of the fault. The fracture frequency used for generating the dual-continuum grid is 1.03 per meter for tsw33 (determined from the fracture map at the alcove floor) and 1.50 per meter for tsw34 (determined from the fracture map at the ceiling of the niche). As shown in Fig. 7, within a cross section of the grid along the

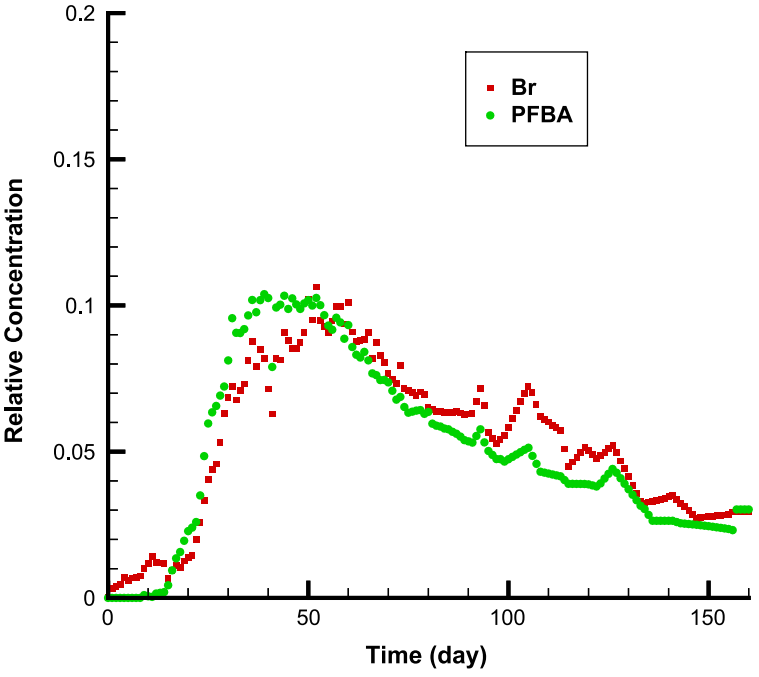

Fig. 6. Observed flux-average breakthrough curve at the niche (Salve et al., 2004).

fault, the grid spacing is 10 cm just above the ceiling of the niche, enabling the seepage process to be accurately simulated. The grid spacings in the direction perpendicular to the fault are 0.024, 0.168, 0.456, 0.756 and 1.44 m, respectively. The smallest spacing is adjacent to the fault, so that water imbibition and tracer diffusion into the fractured rock from the fault can be accurately captured. Cross sections parallel to the fault walls have identical grid meshes (Fig. 7) for different distances from the fault. The niche is represented by an opening at the bottom of the grid (Fig. 7), with the geometry of the opening determined from the survey data of the niche near the fault. Note that this is only an approximation of the geometry of the test site; the actual three-dimensional geometry of the niche with an underground tunnel connected to the niche is difficult to incorporate into the model. However, since our main concern is flow and transport processes within the fault, this geometry representation should be adequate.

Temporally variable inflow rates are imposed on the top boundary, corresponding to the infiltration plot at the alcove floor. (Note that the infiltration plot is only connected to fault elements at the alcove floor in the model.) The side boundary corresponds to zero-flow (in the direction perpendicular to the simulation domain) conditions. The niche wall boundary is modeled by a zero capillary-pressure condition, representing capillary barrier effects (Birkholzer et al., 1999). The bottom boundary was assigned a free-drainage condition. Based on field observations of Flint (1998), matrix saturations are initially assigned to be 0.72 for tsw33 and 0.85 for tsw34. Other initial conditions for the rock mass within the model domain are solute-free and a small water saturation

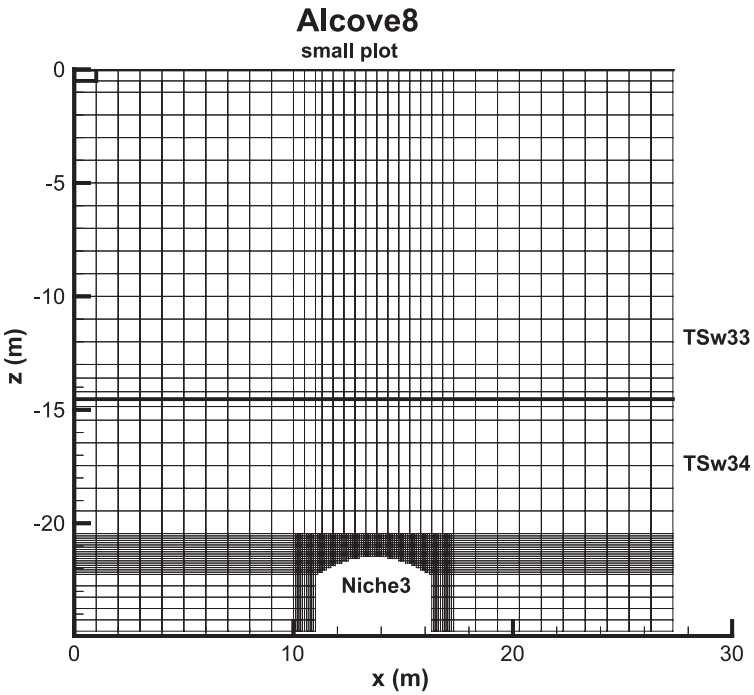

Fig. 7. A vertical cross section of numerical grid.

(1.05e – 2) in both fractures and the fault. Rock properties used in model simulations are presented in the next section.

Model calibration was performed using an inverse modeling code ITOUGH2 (Finsterle, 1997). The model calibration is defined herein as the adjustment of rock hydraulic parameters to make simulation results match the corresponding data. The goodness of match is measured using the standard least squares approach, which minimizes the sum of the squared residuals weighted by the inverse of variance of the data. ITOUGH2 is based on TOUGH2 (Pruess, 1991), which uses the integral-finite-difference method (Narasimhan and Witherspoon, 1976) for spatial discretization, and is a general-purpose simulator for multidimensional, coupled fluid and heat flow of multiphase, multicomponent fluid mixtures in porous and fracture media. A module of TOUGH2, T2R3D (Wu et al., 1996), was used for modeling the tracer transport. T2R3D and ITOUGH2 employ the same procedure and algorithms for modeling liquid flow in fractured rocks, but only ITOUGH2 does inversions and only T2R3D models tracer transport.

4. Model simulations and discussions

The numerical model was first calibrated against the seepage rate at the niche (Fig. 3) and water-travel-velocity data inferred from water arrival times at the boreholes (Fig. 5), to

obtain the calibrated rock properties and the corresponding water flow field. Then, tracer transport simulations with different transport parameters were carried out to evaluate the effects of matrix diffusion and other related processes on solute transport in the fault.

4.1. Calibration of seepage-rate and water-travel-velocity data

Both fracture and matrix properties were assumed to be homogeneous within each geological subunit (tsw33 and tsw34). Fault properties were assumed to be homogeneous within both units. This is based mainly on the following three considerations. First, consideration of the heterogeneity within each subunit would introduce a large number of rock properties that need to be determined by more data than was available from the test site. Second, as previously indicated, similar assumptions have been used by the site-scale model of the unsaturated zone of Yucca Mountain (Bandurraga and Bordvarsson, 1999). It is of interest to examine how well this simple representation of subsurface heterogeneity can be used to model the fault test. Third, a recent study by Zhou et al. (2003) indicates that site-scale flow and transport in the unsaturated zone of Yucca Mountain are mainly determined by large-scale heterogeneity, characterized by property differences between different geological uints, rather than by property variability within a geological unit.

Rock hydraulic properties needed as inputs into the model include fracture and matrix permeabilities, fracture and matrix porosities, fault aperture and permeabilities, Van Genuchten (1980) parameters (for matrix, fractures, and the fault), and the parameter of the active fracture model (Liu et al., 1998), γ, for fractures. The fracture porosities for these two geological units were determined based on both fracture geometry and analyses of gas tracer test data (Liu and Ahlers, 2000). Fracture permeabilities were estimated based on air injection tests performed in the same geological units, and fracture Van Genuchten parameters were estimated using fracture permeability and frequency data (Liu and Ahlers, 2000). The matrix properties were determined based on property data from core measurements (Flint, 1998), and calibrated using matrix saturation and potential data under ambient conditions (Ahlers and Liu, 2000). Because fracture Van Genuchten parameters for tsw33 and tsw34 are similar, a simple average of these parameters was used as the corresponding parameters for the fault. The averaged k/φ (where k is fracture permeability and φ is the corresponding fracture porosity) was calculated as fault permeability. Note that because there is no matrix in the fault in our model (or $\varphi = 1$), the weighted k/φ (rather than weighted k) is employed for estimating fault permeability. The aperture of the fault was initially estimated as the average of fracture apertures of the two subunits. The active fracture model (Liu et al., 1998) parameter γ values for two units, calibrated using the site-scale model of unsaturated zone of Yucca Mountain (Ahlers and Liu, 2000), were used for fractures. (The details of the active fracture model can be found in Liu et al. (1998, 2003c).) Note that the active fracture model was developed for describing fingering flow in fracture networks rather than in a single fracture. Consequently, the active fracture model does not apply to the fault here. In fact, most of the parameter values mentioned above and given in Table 1 are not site-specific for the fault test site. These values were used as initial guesses for model calibration against the seepage-rate and water-travel-velocity data observed from the fault test. To reduce the number of

Table 1
Uncalibrated rock properties

Rock property	Fault	tsw33		tsw34	
		Fracture	Matrix	Fracture	Matrix
Permeability (m^2)	4.34e − 11	5.5e − 13	3.08e − 17	3.5e − 14	4.07e − 18
Porosity	1.00	6.6e − 3	0.154	1.e − 2	0.11
Fracture frequency (m)		1.03		1.5	
Fracture aperture (m)	1.12e − 3	1.49e − 3		7.4e − 4	
Active fracture model parameter γ	0.0	0.41		0.41	
Van Genuchten α (Pa^{-1})	1.0e − 3	1.46e − 3	2.13e − 5	5.16e − 4	3.86e − 6
Van Genuchten *m*	0.608	0.608	0.298	0.608	0.291

variables in model calibration (or inverse modeling), parameters expected to significantly affect simulated water travel time and seepage rate were varied in the calibration, while other parameters were kept unchanged. The varied parameters were fracture and fault permeabilities, fracture porosity, fault aperture, and fracture and fault Van Genuchten α values.

Infiltration-seepage processes in the fault and the surrounding fractured rock were determined by several mechanisms. Liquid water applied at the alcove floor (Fig. 7) flowed first into the fault and then into fractured networks connected to the fault. Matrix imbibition occurred at interfaces between fractures and the matrix and between the fault and the matrix. Water travel time to the rock above the niche ceiling was influenced by fracture porosity, fault aperture, and the matrix imbibition process. When water arrived at the intersection between the fault and the niche, it could not immediately seep into the niche until the capillary pressure became zero because of capillary barrier effects (Philip et al., 1989; Birkholzer et al., 1999). The capillary barrier can divert flow away from the opening, resulting in only a portion of the water arriving at the niche ceiling actually seeping into the niche.

Fig. 8 shows a comparison between niche seepage-rate data and the simulation result from a model calibration (Run #1) without considering the water-travel-velocity data from the boreholes. In this calibration run, fracture porosity and fault aperture were not varied because a preliminary sensitivity study indicated that simulated seepage rates are not significantly sensitive to these parameters. A fairly good match was obtained (Fig. 8); however, water travel velocity is significantly overestimated (Fig. 9). Water travel velocities were calculated from water arrival times at locations about 1 m above the middle of the opening in Fig. 7. In the model, the travel time was defined as the time when fault or fracture saturation was increased from the initial value of 1.05e − 2 to 1.06e − 2. Table 2 gives the calibrated properties obtained from Run #1.

The overestimation of the water travel velocities may result from the following: (1) some cavities in tsw33 are connected to fractures and could contribute to increasing the storage in the fracture continuum; (2) in reality, the fault is a zone rather than a single fracture. The effective aperture from this zone may be much larger than the assumed aperture value for the fault (Table 1). Neither of these factors was considered in Run #1 (first calibration). Taking these factors into consideration, the new calibration (Run #2) allowed both fault aperture and fracture porosity in tsw33 to vary in addition to the

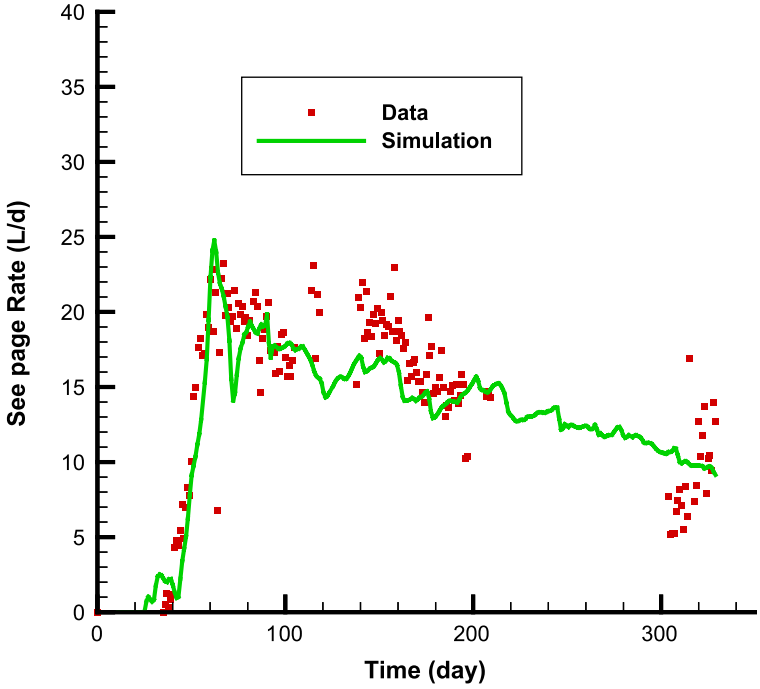

Fig. 8. A comparison between simulated seepage rates as a function of time (Run #1) and field observations at the niche.

properties from Table 2. The resultant values are 3 cm for fault aperture and 0.066 for fracture porosity of tsw33 (Table 3). While the actual width of the fault zone is unknown, the estimated equivalent fault aperture (3 cm) is considered to be acceptable. (The width of the infiltration plot at the alcove floor is about 45 cm.) The estimated fracture porosity is consistent with those estimated from water release tests performed in the same geological unit (Wang, 2002).

Fig. 9 shows a comparison among calculated water travel velocities from two calibration runs and the velocity data observed from the fault test. The simulated water travel velocities from Run #2 are much closer to the observed data than those from Run #1 (especially near the fault). However, the water travel velocities away from the fault are still overestimated. One possible explanation is that matrix imbibition from fractures above the niche were underestimated because the dual-continuum approach considerably underestimates the pressure gradient near a fracture matrix interface during transient flow conditions (Pruess and Narasimhan, 1985; Doughty, 1999). While this problem could be resolved with the multiple interacting continua model of Pruess and Narasimhan (1985), the computational intensity of the inverse model problem under consideration would be significantly increased. Note that a model calibration involves a great number of forward simulation runs. Considering that (1) the transient flow effects would be considerably reduced at later time of the test and that (2) our focus here is on flow and transport within and near fault, simulated flow field and calibrated rock properties from Run #2 were used

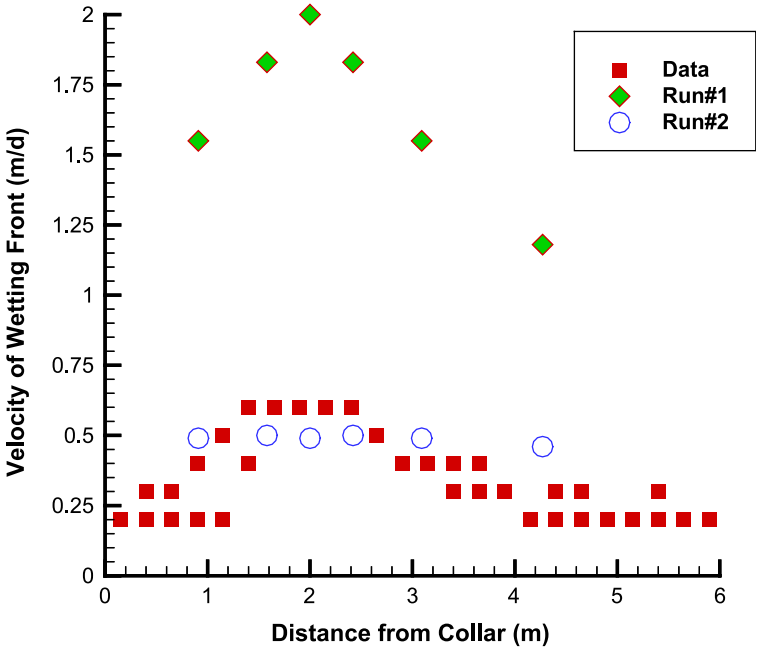

Fig. 9. A comparison among calculated water travel velocities from two calibration runs and the velocity data observed from the fault test.

for simulating tracer transport at the test site. Fig. 10 also shows a comparison between simulated seepage rates as a function of time (Run #2) and field observations. The match is reasonable.

4.2. Effects of matrix diffusion

Tracer transport within the fault is controlled by several processes, including advection, diffusion into the matrix blocks (matrix diffusion), mass exchange between the fault and the surrounding fracture networks, and dispersion. Our special attention in this study is given to evaluating the relative importance of matrix diffusion. To do so, we used the flow field obtained from Run #2 to simulate tracer transport processes and compare simulation results with field observations (Fig. 6).

Two conservative tracers with different molecular diffusion coefficients ($2.08e-9$ m^2/s for Br and $7.60e-10$ m^2/s for PFBA) were used in the fault test. The effective diffusion

Table 2
Rock properties calibrated from seepage-rate data (Run #1)

Rock property	Fault	tsw33	tsw34
Fracture permeability (m^2)	$6.67e-11$	$8.93e-13$	$3.16e-14$
Fracture Van Genuchten α (Pa^{-1})	$1.15e-3$	$1.67e-3$	$4.59e-4$

All the other rock properties are the same as those in Table 1.

Table 3
Rock properties calibrated from both seepage-rate and water-travel-velocity data (Run #2)

Rock property	Fault	tsw33	tsw34
Fracture permeability (m^2)	1.12e – 10	1.23e – 12	5.01e – 13
Fracture porosity		0.066	
Fracture aperture (m)	0.03		
Fracture Van Genuchten α (Pa^{-1})	1.24e – 3	2.19e – 3	1.09e – 3

All the other rock properties are the same as those in Table 1.

coefficient for the matrix diffusion process is the product of the molecular diffusion coefficient and tortuosity factor. Based on analyses of the relevant diffusion experiment results for tuff matrix samples in the unsaturated zone of Yucca Mountain, Moridis and Hu (2000) concluded that the tortuosity factor for the tuff matrix could be approximated by the corresponding matrix porosity. As a consequence, the average matrix porosity for tsw33 and tsw34 (0.13) was used as the tortuosity factor.

Fig. 11 shows comparisons between simulated breakthrough curves at the niche for two different fault–matrix and fracture–matrix interface areas and the observed data. One simulation corresponds to an interface area defined in the original numerical grid, which considers the fault as a fracture-like feature with two vertical walls, while the other simulation corresponds to an enhanced interface area (corresponding to an

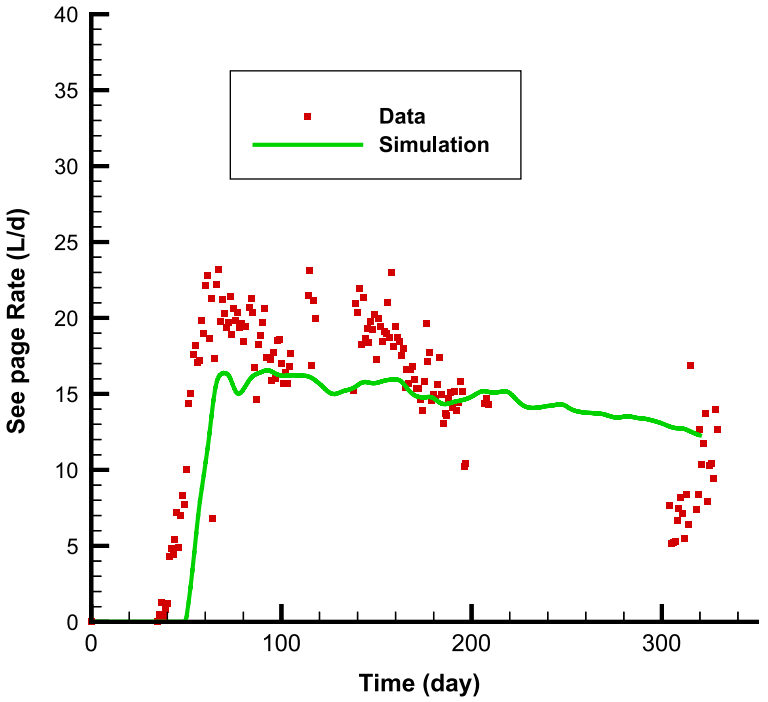

Fig. 10. A comparison between simulated seepage rates at the niche as a function of time (Run #2) and field observations.

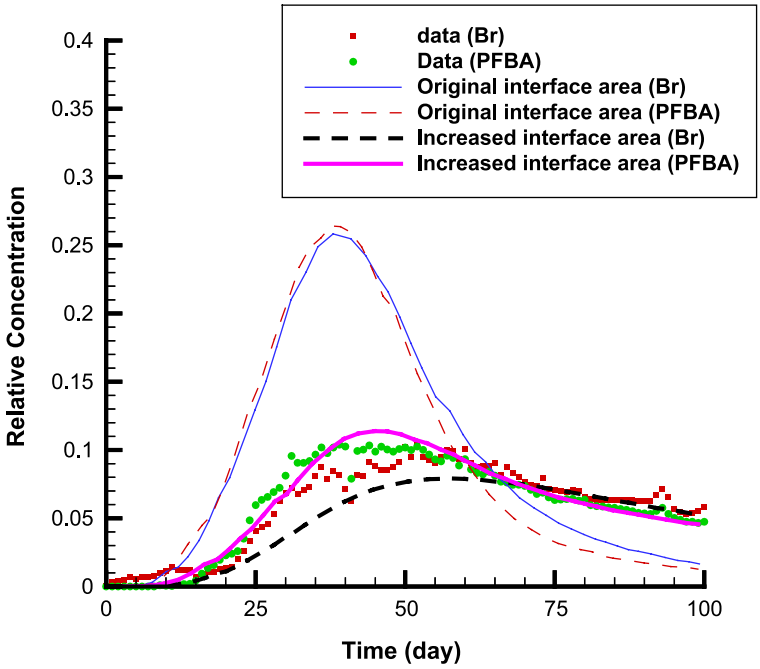

Fig. 11. Comparisons between simulated breakthrough curves at the niche for two different fault–matrix interface areas and the observed data.

effective matrix diffusion coefficient increased by 45 times over that in the first simulation). In these two simulations, the dispersivity is assumed to be zero. (The relative importance of the dispersion will be discussed later.) Since the diffusive flux from the fault and the fractures to the matrix is related to the matrix diffusion coefficient and the fault–matrix (and fracture–matrix) interface area, changes in the interface area for a given matrix diffusion coefficient are equivalent to changes in matrix diffusion coefficient for a given interface area. For simplicity, the matrix diffusion coefficient value was changed in actual simulations, and the numerical grid (defining the interface area) was kept unchanged. Note that changes in the interface area should not significantly alter the flow field during the period of the tracer test. Tracers were introduced into infiltrating water at about 200 days after infiltration started, resulting in the matrix near the fault being almost saturated during the tracer test and the matrix imbibition being insignificant. As shown in Fig. 11, the simulated breakthrough curve with the original interface area is very different from the observed data. It exhibits much larger concentration peak values and much earlier arrival times for these peaks. The observed data are favorably matched by the simulated result with increased interface area, indicating that matrix diffusion significantly affects the overall solute transport behavior and is underestimated by the simulation using the original interface area.

The need to increase interface areas between fractures (and faults) and the matrix (or effective matrix diffusion coefficient) in matching the field observations of tracer

transport in fractured rock has been recently reported by several researchers. Shapiro (2001) reported an interpretation of concentration measurements for tritium and dichlorodifluoromethane collected from a glacial drift and fractured crystalline rock over 4 km^2 in central New Hampshire. He found that the effective diffusion coefficient at the kilometer scale is at least three orders of magnitude greater than laboratory estimates of diffusion in crystalline rock. Neretnieks (2002) presented comparisons between several analytical solutions with tracer test results (with a test scale of 5 m) at the Äspö site in Sweden and reported a need for a factor 30–50 times larger fracture–matrix interface area than expected to match the test data. He also indicated that nine other research groups reached a similar conclusion in their interpretation of the same test data set. Liu et al. (2003b) reported a model interpretation of infiltration and tracer test (with a test scale of 30 m) in a densely fractured rock, suggesting that the match to the tracer concentration data with the corresponding simulation result requires the fracture–matrix interface area to be increased by a factor of four. Our results in this study are consistent with these previous findings. Note that the increased matrix diffusion coefficients (or fracture–matrix and fault–matrix interface areas) may be different between the fault zone and the surrounding fractured rock. For simplicity, the same (increased) matrix diffusion coefficients were used in this study for both the fault zone and the surrounding fractured rock, considering that the breakthrough curves observed from the intersection between the fault and the niche ceiling are expected to be mainly influenced by tracer transport in the fault zone.

Several mechanisms regarding the increase in the interface area (or effective matrix diffusion coefficient) have been reported in the literature. They include (1) advective mass exchanges from high-permeability fractures to low-permeability fractures (Shapiro, 2001), (2) diffusion into stagnant water zones (Neretnieks, 2002), (3) effects of complex fractures that were often regarded as single fractures in model studies, but actually consist of a group of adjacent and connected subfractures (Tsang and Doughty, 2003), and (4) enhanced fracture–matrix interface areas for fractures with small-trace lengths that do not contribute to global flow and are not considered in the survey data (and therefore in the dual-continuum numerical grid) (Wu et al., 2004; Liu et al., 2003a,b). In addition to these potential mechanisms, two other factors also contribute to the increase in the interface area. First, in the relevant analytical and numerical solutions to tracer transport, fracture walls are generally assumed to be flat. However, it is now well known that fracture walls are rough and characterized by fractal geometry (National Research Council, 1996). Consequently, the actual interface areas between fractures (faults) and the matrix are larger than what are calculated using flat fracture walls. Second, a fault zone may include a great number of crushed matrix blocks that have smaller sizes than the fracture spacing in a nonfault zone. These crushed matrix blocks can make a significant contribution to the matrix diffusion within the fault, but are not considered in our numerical grid, where the fault is simply treated as a vertical fracture. To compensate for the effects of these mechanisms mentioned above, an increase in fault–matrix interface area is obviously needed.

Although simulation results with the increased interface area reasonably match the observed data (Fig. 11), the concentration difference (resulting from different molecular diffusion coefficients) at a given time for the two tracers is generally overestimated by the

model. One plausible explanation is that the crushed matrix blocks within the fault zone have much smaller sizes (or fracture spacings) than those in the surrounding fractured rock. This, however, is not considered in our model. The smaller sizes require shorter times for equilibration of tracer concentration between the center and outer surface of a matrix block, reducing the difference between the effects of matrix diffusion on overall solute transport behavior for different molecular-diffusion coefficients. This issue was not further explored in the current modeling study because the matrix block size distribution within the fault cannot be independently estimated or observed. However, we acknowledge that this interesting issue may need to be further investigated in the future, when the data on the matrix block sizes (or fracture spacings) within a fault are available.

Compared with matrix diffusion, the macro dispersion process is not considered to be significant within the fault (and surrounding fracture networks) for this particular test. Field measurements indicate that the water-travel-velocity distribution is rather uniform within and near the fault (Fig. 5), whereas macrodispersion results from variability in water velocity. This is further confirmed by observed breakthrough curves from three flow paths within the fault (Salve et al., 2004). They have similar arrival times of peak concentrations (Salve et al., 2004). These experimental observations are consistent with the findings from our model analyses: the observed data are very difficult to match when a considerable degree of dispersion is included in the model. For example, Fig. 12 shows simulated breakthrough curves with a longitudinal

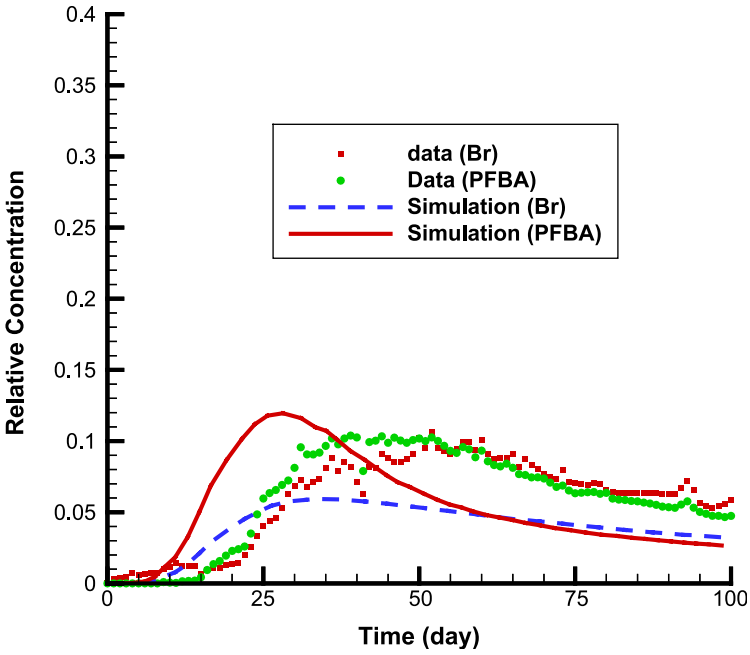

Fig. 12. Comparisons between simulated breakthrough curves (considering dispersion) at the niche for the increased fault–matrix interface areas and the observed data.

dispersivity value of 1 m and a transverse dispersivity value of 0.1 m for fault and fractures (and with the increased fault–matrix and fracture–matrix interface areas), compared to results in Fig. 11 (without considering dispersion). Unlike tracer transport in a single continuum, larger dispersivity values generally correspond to earlier arrival times of peak concentrations and to a larger difference between these peak concentrations for the two different tracers as a result of a combination of effects of matrix diffusion and dispersion.

4.3. Implication for radionuclide transport in the unsaturated zone of Yucca Mountain

The Yucca Mountain site (where the fault test was carried out) is the proposed geological disposal site for high-level nuclear waste in the United States. Radionuclide transport from the repository horizon to the water table is a key factor affecting the performance of the proposed repository. The study results herein have some important implications for the performance assessment of the proposed site.

Matrix diffusion has been identified as a key mechanism for retarding the radionuclide transport in both unsaturated and saturated fractured rock (e.g., Bodvarsson et al., 2001; Neretnieks, 1980, 2002). An increase of the fracture (and fault)–matrix interface area (or effective matrix-diffusion coefficient) seems to be common for matching field-scale solute transport observations, as suggested by this study and previous studies (Shapiro, 2001; Neretnieks, 2002; Liu et al., 2003a). Although some physical explanations for this increase are available, as discussed in Section 4.2, more detailed studies of the associated mechanisms are needed to confirm these explanations. The current site-scale model for the unsaturated zone of Yucca Mountain (Wu et al., 2002; Moridis and Hu, 2000) does not consider the effects of this enhancement. Consequently, the radionuclide travel time from the proposed repository to the water table, estimated based on the site-scale model, may be underestimated.

The other related issue is the effects of lithophysal cavities (existing in several geological layers at the Yucca Mountain site) on water flow and radionuclide transport processes. One may intuitively expect the cavities connected to fractures to act as capillary barriers under unsaturated conditions, because the cavity openings are much larger than fracture apertures. However, both this study and analyses of water release tests performed in the related geological units at the Yucca Mountain site (Wang, 2002) suggest that cavities are accessible by water within fracture networks, and therefore retard the downward water flow and radionuclide transport processes. This is also supported by a field observation that mineral coatings exist in many cavities (Whelan et al., 2002). The coating is a signature for liquid–water flow paths. Although the cavity openings are larger than fracture apertures, the roughness of cavity walls could result in film flow (along cavity walls) from fractures to the cavities (Tokunaga and Wan, 1997). (This existence of film flow within cavities may still be an issue of debate (e.g.,Whelan et al., 2002).) The effects of cavities are also not considered in the site-scale model for the unsaturated zone of Yucca Mountain. This omission would result in further underestimating the radionuclide travel time from the proposed repository to the water table.

5. Concluding remarks

A three-dimensional numerical model was developed for analyzing the results of an infiltration and tracer test in a fault, performed by Salve et al. (2003), in the unsaturated zone of Yucca Mountain, Nevada. Within the model, the fault was represented as a vertical fracture-like feature and the surrounding rock was treated as dual continua (fractures and matrix).

Model calibration against the seepage and water-travel-velocity data suggests that the lithophysal cavities connected to fractures can considerably enhance the effective fracture porosity and therefore retard water flow in fractures. Comparisons between simulation results and the tracer concentration data indicate that matrix diffusion is an important mechanism for solute transport in unsaturated fractured rock. An increased fault–matrix interface area is found to be needed for matching the observed tracer data. This is consistent with previous studies reported in the literature. The relative importance of the dispersion process within the fracture network in the test is found to be small.

The results from this study imply that the current site-scale model for the unsaturated zone of Yucca Mountain may underestimate solute transport time within the unsaturated zone because an increased fracture–matrix interface area and potential effects of the lithophysal cavities are not considered in the site-scale model. However, we acknowledge that the applicability of these results (from a 20 m scale test) in the larger site-scale transport processes may need further investigation.

Acknowledgements

We are indebted to Q. Zhou and D. Hawkes at Lawrence Berkeley National Laboratory for their careful review of a preliminary version of this manuscript. We also appreciate the constructive review comments from Drs. Christine Doughty at Lawrence Berkeley National Laboratory and Joseph F. Whelan at Geological Survey. This work was supported by the Director, Office of Civilian Radioactive Waste Management, U.S. Department of Energy, through Memorandum Purchase Order EA9013MC5X between Bechtel SAIC Company, LLC, and the Ernest Orlando Lawrence Berkeley National Laboratory (Berkeley Lab). The support is provided to Berkeley Lab through the U.S. Department of Energy Contract No. DE-AC03-76SF00098.

References

Ahlers, C.F., Liu, H.H., 2000. Calibrated Properties Model. CRWMS M&O, Las Vegas, NV Rep. MDL-NBS-HS-000003.

Bandurraga, T.M., Bordvarsson, G.S., 1999. Calibrating hydrogeologic parameters for the 3-D site-scale unsaturated zone model of Yucca Mountain, Nevada. J. Contam. Hydrol. 38, 46–47.

Birkholzer, J., Li, G., Tsang, C.F., Tsang, Y., 1999. Modeling studies and analysis of seepage into drifts at Yucca Mountain. J. Contam. Hydrol. 38, 349–384.

Bodvarsson, G.S., Tsang, Y. (Eds.), 1999. Yucca Mountain Project. J. Contam. Hydrol., vol. 38, pp. 1–146.

Bodvarsson, G.S., Liu, H.H., Ahlers, R., Wu, Y.S., Sonnethal, E., 2001. Parameterization and upscaling in

modeling flow and transport at Yucca Mountain, in Conceptual Models of Flow and Transport in the Fractured Vadose Zone, National Research Council, National Academy Press, Washington, DC.

Doughty, C., 1999. Investigation of conceptual and numerical approaches for evaluating moisture, gas, chemical and heat transport in fractured rock. J. Contam. Hydrol. 38, 69–106.

Finsterle, S., 1997. ITOUGH2 Command Reference, Version 3.1, Rep. LBNL-40041. Lawrence Berkeley National Laboratory, Berkeley, CA.

Flint, L.E., 1998. Characterization of Hydrogeologic Units Using Matrix Properties, Yucca Mountain, Nevada, Water Resour. Invest. Rep. 97-4243. U.S. Geological Survey, Denver, CO.

Foster, S.S.D., 1975. The chalk groundwater tritium anomaly: a possible explanation. J. Hydrol. 25, 159–165.

Jardine, P.M., Sanford, W.E., Gwo, J.P., Reedy, O.C., Hicks, D.S., Riggs, J.S., Bailey, W.B., 1999. Quantifying diffusive mass transfer in fractured shale bedrock. Water Resour. Res. 35 (7), 2015–2030.

Liu, H.H., Ahlers, C.F., 2000. Analysis of Hydrologic Properties Data, Rep. MDL-NBS-HS-000002, CRWMS M&O, Las Vegas, NV.

Liu, H.H., Doughty, C., Bodvarsson, G.S., 1998. An active fracture model for unsaturated flow and transport in fractured rocks. Water Resour. Res. 34 (10), 2633–2646.

Liu, H.H., Bodvarsson, G.S., Finsterle, S., 2003a. A Note on unsaturated flow in two-dimensional fracture networks. Water Resour. Res. 38 (9), 1176 (doi:10.1029/2001WR000977).

Liu, H.H., Haukwa, C.B., Ahlers, F., Bodvarsson, G.S., Flint, A.L., Guertal, W.B., 2003b. Modeling flow and transport in unsaturated fractured rocks: an evaluation of the continuum approach. J. Contam. Hydrol. 62–63, 173–188.

Liu, H.H., Zhang, G., Bodvarsson, G.S., 2003c. The active fracture model: its relation to fractal flow patterns and an evaluation using field observations. Vadose Zone Journal 2, 259–269.

McKenna, S.A., Meigs, L.C., Haggerty, R., 2001. Tracer tests in a fractured dolomite: 3. Double-porosity, multiple-rate mass transfer processes in convergent flow tracer tests. Water Resour. Res. 37 (5), 1143–1154.

Meigs, L.C., Beauheim, R.L., 2001. Tracer tests in a fractured dolomite: 1. Experimental design and observed tracer recoveries. Water Resour. Res. 37 (5), 1113–1128.

Moreno, L., Gylling, B., Neretnieks, I., 1997. Solute transport in fractured media—the important mechanisms for performance assessment. J. Contam. Hydrol. 25, 283–298.

Moridis, G., Hu, Q., 2000. Radionuclide Transport Model Under Ambient Conditions. CRWMS M&O, Las Vegas, NV Rep. MNL-NBS-HS-000008.

Narasimhan, T.N., Witherspoon, P.A., 1976. An integrated finite difference method for analyzing fluid flow in porous media. Water Resour. Res. 12, 57–64.

National Research Council, 1996. Rock Fractures and Fluid Flow, Contemporary Understanding and Applications. National Academy Press, Washington, DC.

Neretnieks, I., 1980. Diffusion in the rock matrix: an important factor in radionuclide retardation? J. Geophys. Res. 85, 4379–4397.

Neretnieks, I., 2002. A stochastic multi-channel model for solute transport-analysis of tracer tests in fractured rock. J. Contam. Hydrol. 55, 175–211.

Ostensen, R., 1998. Tracer tests and contaminant transport rates in dual-porosity formations with application to WIPP. J. Hydrol. 204, 197–216.

Philip, J.R., Knight, J.H., Waechter, R.T., 1989. Unsaturated seepage and subterranean holes: conspectus, and exclusion problem for cylindrical cavities. Water Resour. Res. 25 (1), 16–28.

Phillips, F.M., 2001. Investigating flow and transport in the fractured vadose zone using environmental tracers, in Conceptual Models of Flow and Transport in the Fractured Vadose Zone, National Research Council, National Academy Press, Washington, DC.

Pruess, K., 1991. TOUGH2—A General Purpose Numerical Simulator for Multiphase Fluid and Heat Flow. Lawrence Berkeley National Laboratory, Berkeley, CA. Rep. LBNL-29400.

Pruess, K., 1999. A mechanistic model for water seepage through thick unsaturated zones in fractured rocks of low matrix permeability. Water Resour. Res. 35 (4), 1039–1051.

Pruess, K., Narasimhan, T.N., 1985. A practical method for modeling fluid and heat flow in fractured porous media. Soc. Pet. Eng. J. 25 (1), 14–16.

Salve, R., Oldenburg, C.M., 2001. Water flow within a fault in altered nonwelded tuff. Water Resour. Res. 37 (12), 3043–3056.

Salve, R., Liu, H.H., Wang, J.S.Y., Hudson, D., 2004. Development of wet plume following liquid release along a fault. Water Resour. Res. (in review).

Seol, Y., Liu, H.H., Bodvarsson, G.S., 2003. Effects of dry fractures on matrix diffusion in unsaturated fractured rocks. Geophys. Res. Lett. 30 (2), 1075 (doi: 10.1029/2002GL016118).

Shapiro, A.M., 2001. Effective matrix diffusion in kilometer-scale transport in fractured crystalline rock. Water Resour. Res. 37 (3), 507–522.

Tokunaga, T.K., Wan, J., 1997. Water film flow along fracture surface of porous rock. Water Resour. Res. 33, 1287–1295.

Tsang, Y.W., Birkholzer, J.T., 1999. Prediction and observations of the thermal–hydrological conditions in the single heater test. J. Contam. Hydrol. 38, 385–425.

Tsang, C.F., Doughty, C., 2003. A particle-tracking approach to simulating transport in a complex fracture. Water Resour. Res. 39 (7), 1174 (doi:10.1029/2002WR001614).

Van Genuchten, M., 1980. A closed-form equation for predicting the hydraulic conductivity of unsaturated soil. Soil Sci. Soc. Am. J. 44 (5), 892–898.

Wang, J.S.Y., 2002. In situ field testing of processes. BSC, Las Vegas, NV. Rep. ANL-NBS-HS-000005.

Wang, J.S.Y., Narasimhan, T.N., 1993. Unsaturated flow in fractured porous media. In: Bear, J., Tsang, C.-F., de Marsily, G. (Eds.), Flow and Contaminant Transport in Fractured Rock. Academic Press, San Diego, CA.

Wang, J.S.Y., Trautz, R.C., Cook, P.J., Finsterle, S., James, A.L., Birkholzer, J., 1999. Field tests and model analyses of seepage into drift. J. Contam. Hydrol. 38, 232–347.

Whelan, J.F., Paces, J.B., Peterman, Z.E., 2002. Physical and stable-isotope evidence for formation of secondary calcite and silica in the unsaturated zone, Yucca Mountain, Nevada. Appl. Geochem. 17, 735–750.

Wu, Y.S., Ahlers, C.F., Fraser, P., Simmons, A., Pruess, K., 1996. Software qualification of selected TOUGH2 modules. Lawrence Berkeley National Laboratory, Berkeley, CA. LBNL-39490.

Wu, Y.S., Pan, L., Zhang, W., Bodvarsson, G.S., 2002. Characterization of flow and transport processes within the unsaturated zone of Yucca Mountain, Nevada, under current and future climates. J. Hydrol. 54, 215–247.

Wu, Y.S., Liu, H.H., Bodvarsson, G.S., 2004. A triple-continuum model for investigating effects of small-scale fractures on flow and transport processes in fractured rocks. J. Contam. Hydrol. (in press).

Zhou, Q., Liu, H.H., Bodvarsson, G.S., Oldenburg, C.M., 2003. Flow and transport in unsaturated fractured rock: effects of multiscale heterogeneity of hydrogeologic properties. J. Contam. Hydrol. 60, 1–30.